NJC

ROYAL SOCIETY OF CHEMISTRY

PAPER

View Article Online
View Journal | View Issue

Cite this: *New J. Chem.*, 2021, **45**, 7315

A smart mitochondria-targeting TP-NIR fluorescent probe for the selective and sensitive sensing of H_2S in living cells and mice†

Qiaomei Yang,[a] Liyi Zhou, *[a] Longpeng Peng,[a] Gangqiang Yuan,[a] Haiyuan Ding,[a] Libin Tan[a] and Yizhuang Zhou*[b]

Received 19th February 2021,
Accepted 17th March 2021

DOI: 10.1039/d1nj00840d

rsc.li/njc

Hydrogen sulfide (H_2S) is one of the important gaseous signalling molecules, which plays key roles in various critical biological processes. In this work, we report a novel two-photon near-infrared (TP-NIR) fluorescent probe (**MNIR-H_2S**) for the sensing of mitochondrial H_2S in living cells, tissues, zebrafish and nude mice. Using a xanthene dye as a TP-excitation (810 nm) NIR-emission (668 nm) fluorophore, a well-known H_2S response moiety with a robust intramolecular charger transfer (ICT) effect can quickly respond to H_2S and effectively quench the fluorescence intensity, and an oxonium cation structure serves as a mitochondria-targeting site. Notably, **MNIR-H_2S** displays high sensitivity, high selectivity, low cytotoxicity, powerful mitochondrial localization ability, deep tissue penetration, and a very minimal imaging background. Biological imaging results show the biological application of **MNIR-H_2S** as a robust new tool for use in H_2S imaging in biological systems.

Introduction

Hydrogen sulfide (H_2S) is notorious for having a strong smell that resembles rotten eggs, and has traditionally been misunderstood to be just a toxic gas. However, a number of current studies have indicated that H_2S has certain biological functions due to its typical concentration in the blood being the range of 10–100 μM. Indeed, current studies regard H_2S as the third gaseous signalling molecule that is present in living biological systems, followed by carbon monoxide (CO) and nitric oxide (NO).[1] H_2S has been thought to be related to various physiological processes, such as vasodilation, antioxidation, anti-apoptosis, anti-inflammation.[2] Moreover, it plays the role of an antioxidant and reactive oxygen species (ROS) scavenger *in vivo*. In addition, studies have indicated that its deregulation could be related to the development and occurrence of certain diseases, such as liver cirrhosis,[3] diabetes,[4] Down's syndrome,[5] and Alzheimer's disease.[6] Although H_2S has been recognized to be related to various physiological and pathological functions, some potential molecular events remain unclear. Therefore, the development of accurate and reliable methods to understand the biological roles of H_2S and its high biocompatibility and site-specificity is urgently required.

Nowadays, several analytical methods (such as colorimetry and electrochemical analysis, gas chromatography and sulfide precipitation) are used to detect H_2S, but these usually require complex pretreatment of samples, so they are often difficult to use for *in vivo* detecting and imaging.[7] Compared with the above analytical methods, fluorescence imaging is considered a robust tool for sensing and monitoring some biomolecules *in vivo* due to its outstanding performance, including high sensitivity, good selectivity, fast response, less bio-damage, and real-time imaging. To date, many H_2S fluorescent probes have been reported. However, most of them are one-photon (OP) fluorescent probes, which use short-wavelength of ultraviolet-visible light excitation and emission to cause photobleaching and shallow tissue imaging. In addition, most of them do not have organelle targeting groups with which to target organelles to provide quantitative analytical information of H_2S at the organelle level. Therefore, this limits their application *in vivo* to investigate the links between H_2S and physiology and pathology.[8] In contrast, two-photon near-infrared (TP-NIR) fluorescent probes adopt two photons of NIR laser pulse excitation and NIR emission, which have many advantages in biological imaging, such as high spatial resolution, deep imaging depth, good three-dimensional spatial localization effects, decreasing of photodamage to biological samples, and the elimination of autofluorescence.[9,10] More importantly,

[a] *Hunan Key Laboratory of Processed Food for Special Medical Purpose, National Engineering Laboratory for Deep Process of Rice and Byproducts, College of Food Science and Engineering, Central South University of Forestry and Technology, Changsha, Hunan 410004, China. E-mail: zhouly0817@163.com*
[b] *Guangxi Key Laboratory of Tumor Immunology and Microenvironmental Regulation, Guilin Medical University, Guilin, Guangxi 541001, China. E-mail: zhouyizhuang3@163.com*

† Electronic supplementary information (ESI) available. See DOI: 10.1039/d1nj00840d

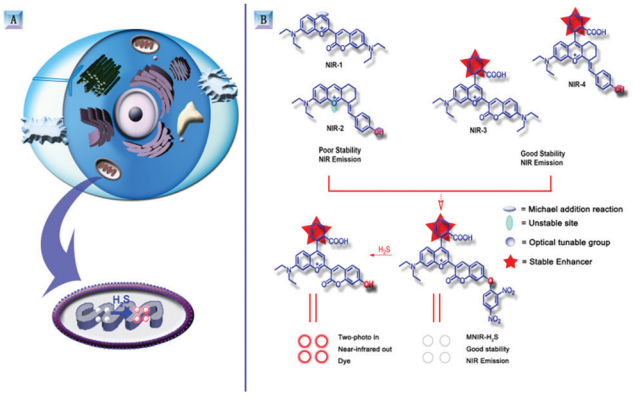

Scheme 1 (A) Proposed mechanism for the sensing of H_2S in mitochondria when using the TP-NIR fluorescent probe **MNIR-H_2S**. (B) Modification of previously reported unstable (NIR-1, NIR-2) and stable (NIR-3, NIR-4) dyes to construct the new stable TP-NIR H_2S fluorescent probe **MNIR-H_2S**.

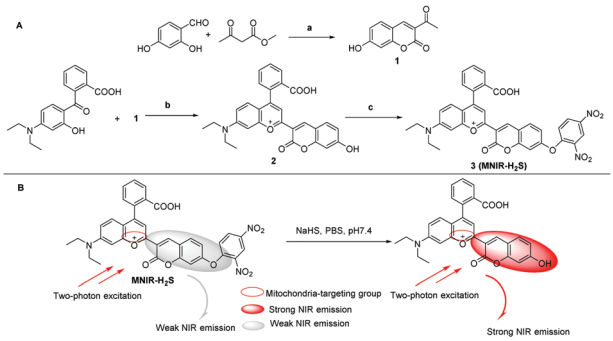

Fig. 1 (A) Synthesis steps of the TP-NIR fluorescent probe **MNIR-H_2S**: a, EtOH, piperidine, 80 °C, 4 h; b, concentrated sulfuric acid, 90 °C, 8 h; c, 2,4-dinitrofluorobenzene, CH_2Cl_2, triethylamine, 3 h. (B) Response mechanism of the mitochondrial TP-NIR fluorescent probe toward hydrogen sulfide.

compared with fluorescent probes without organelle targeting groups, organelle-targeted fluorescent probes can accurately, quickly and conveniently obtain H_2S information at the organelle level, and provide a theoretical basis and technical support for the early diagnosis and treatment of H_2S-related diseases. Therefore, there is an urgent need to develop organelle-targeted TN-NIR fluorescent probes for the detection and imaging of H_2S in biological systems Scheme 1.

In order to overcome these challenging bottlenecks, in this work, taking previously reported unstable TP excitation NIR emission fluorescent dyes,[11] we rationally modified their structure to obtain a new TP-excited (810 nm) NIR emission (668 nm) mitochondria-targeting fluorescent probe **MNIR-H_2S** for the sensing of H_2S in living cells, tissues and nude mice. In this new scaffold, an *o*-carboxyphenyl group was employed to occupy the para-position of the oxonium cation and prevent a Michael addition reaction, and also prevent the pH-triggered oxonium cation ring-opening reaction. Notably, in this new fluorescent probe, the oxonium cation serves as a mitochondria-targeting moiety, and the well-known H_2S response moiety 2,4-dinitrophenyl ether (DBN)[12] has a strong ICT effect to quench NIR fluorescence intensity at 668 nm. In the presence of H_2S, the TP-NIR fluorophore shows a "turn-on" fluorescence intensity at 668 nm, and the fluorescence intensity increases by ~150 fold. This new fluorescent probe exhibits outstanding selectivity and sensitivity for the sensing of H_2S both *in vitro* and *in vivo*. Impressively, the biological images showed that this new probe can be successfully applied for the sensing of H_2S in living HeLa cells, onion tissue, zebrafish and nude mice.

Experimental section

Materials and apparatus

The materials and equipment used are described in the ESI.†

Synthesis and characterization of MNIR-H_2S

The synthesis of the fluorescent H_2S probe **MNIR-H_2S** is shown in Fig. 1A. The classical ssyntheses of **1** and **2** were carried out according to the methods described in the literature[13] or modifications of these procedures. For the synthesis of **2**: 313 mg (1 mmol) of 2-[4-(diethylamino)-2-hydroxybenzoyl]benzoic acid, 204 mg (1 mmol) of **1**, and 15 mL of concentrated sulfuric acid were added into a single-neck round-bottom flask equipped with a condenser, and the reaction temperature was slowly raised to 90 °C, the temperature at which the mixture was stirred for 8 h. After being allowed to cool, the reaction solution was poured into 100 mL of ice-water, and then 3 mL of perchloric acid ($HClO_4$) was added into the mixture solution. The resulting purple-black solid was filtered off under reduced pressure, washed with cooled water (3 × 10 mL), and dried to obtain the crude product. Finally, the crude product was further purified by column chromatography (CH_2Cl_2/CH_3OH = 50 : 1, v/v) to obtain the target compound as a black solid in 85.3% yield. ^{1}H NMR (400MHz, d6-DMSO): 11.85 (s, 1H), 8.89 (s, 1H), 8.13 (s, 1H), 7.95–7.93 (t, J = 4.00Hz, 1H), 7.79–7.69 (d, J = 20.00Hz, 3H), 7.38–7.37 (d, J = 4.00Hz, 1H), 6.71 (s, 1H), 6.51 (s, 3H), 6.41 (s, 1H), 4.36 (s, 1H), 1.93–1.90 (q, J = 3.00Hz, 4H), 1.08–1.04 (t, J = 8.00Hz, 6H); 13C NMR (100MHz, d6-DMSO) δ(ppm): 172.59, 169.19, 158.68, 150.02, 149.66, 135.93, 128.55, 127.73, 126.77, 125.28, 124.61, 110.41, 103.84, 97.72, 56.49, 44.27, 21.58, 12.87; LC-MS: m/z $[C_{29}H_{24}NO_6]^+$ calcd 482.51, found 482.52.

One-pot synthesis of the H_2S fluorescent probe MNIR-H_2S (3):

A mixture of 582 mg (1 mmol) of $([C_{29}H_{24}NO_6] + ClO_4^-)_2$, 186 mg (1 mmol) of 2,4-dinitrofluorobenzene, 3 mL of triethylamine, and 50 mL of CH_2Cl_2 were added into a single-neck round-bottom flask equipped with a condenser, and the reaction temperature was slowly raised to 45 °C, at which temperature the reaction was stirred for 3 h. After the completion of the reaction, the mixture was allowed to cool to room temperature, and the solvent was evaporated *in vacuo* using a rotary evaporator to give the crude product as a black solid. Finally, the crude product was further purified by column chromatography (CH_2Cl_2:CH_3OH = 50 : 1, v/v) to obtain the probe **MNIR-H_2S** as a black solid in 85.8% yield. ^{1}H NMR (400MHz, d6-DMSO): 9.08 (s,1H), 8.87–8.86 (d, J = 4.00Hz, 1H), 8.50 (s, 1H), 8.44–8.40 (q, J = 4.00Hz, 1H), 7.96–7.94 (d, J = 8.00Hz, 1H), 7.79–7.68 (m, 2H), 7.47

(s, 1H), 7.40–7.38 (d, J = 8.00Hz, 1H), 7.10–7.07 (d, J = 12.00Hz, 1H), 6.74 (s, 1H), 6.51–6.48 (d, J = 12.00Hz, 4H), 3.40–3.37 (q, J = 3.00Hz, 4H), 1.16–1.12 (t, J = 4.00Hz, 6H); 13C NMR (100MHz, d6-DMSO) δ(ppm): 169.17, 157.33, 156.18, 154.53, 153.56, 152.48, 149.57, 146.19, 141.60, 139.43, 137.97, 130.67, 129.59, 126.00, 121.96, 118.22, 116.87, 110.67, 104.45, 83.21, 46.04, 44.24, 19.03, 12.87; LC-MS: m/z $[C_{35}H_{26}N_3O_{10}]^+$ calcd 648.60, found 648.61.

Spectrophotometric measurements

Fluorescence spectroscopy measurements were carried out in phosphate-buffered solution (PBS, 10 mM) in dimethyl sulfoxide (DMSO) as a co-solvent solution (H_2O/DMSO = 99 : 1, v/v). The pH value of the PBS solution used was from 3.0 to 8.0, which was achieved by adding minimal volumes of HCl or NaOH solutions. Fluorescence emission spectra were recorded at an excitation wavelength of 622 nm in an emission wavelength range from 630 to 800 nm. A 1 mM stock solution of the **MNIR-H_2S** probe was prepared by dissolving **MNIR-H_2S** in DMSO. The procedure for the calibration measurements of **MNIR-H_2S** in the buffer with different H_2S concentrations was as follows: 2 μL of a stock solution of **MNIR-H_2S** and 1996 μL of PBS buffer solution with 2 μL of different H_2S concentration solutions were combined to afford test solutions of 1 μM of **MNIR-H_2S**. Solutions of the various test species were prepared from KCl, $CaCl_2$, NaCl, $MgCl_2$, $ZnCl_2$, $FeCl_3$, $CuSO_4$, $Hg(NO_3)_2$, $PbCl_2$, glutathione (GSH), cysteine (Cys), and glutamate (Glu), using twice-distilled water, with final concentrations of 100 μM. The procedure for the selectivity experiments was as follows. For cations or anions, 2 μL of a stock solution of **MNIR-H_2S**, 1798 μL of PBS solution (pH 7.4) and 200 μL of solutions of each relevant species were combined to afford test solutions, containing 1 μM of **MNIR-H_2S** and 100 μM of the relevant species.

Cytotoxicity assays and imaging

HeLa cells at 1 × 106 cells/well were seeded at varying density in a 96-well plate and incubated overnight. After that, they were incubated with increasing concentrations of **MNIR-H_2S** (0–12 μM) for 24 h. The MTT assay method was then used to assess the cytotoxic effects of **MNIR-H_2S**. Before the fluorescence imaging, the cells were washed three times with 10 mM of PBS (pH7.4), followed by incubating them with 1.0 μM of **MNIR-H_2S** for 30 min (10 mM PBS, 1% DMSO) at 37 °C and they were then washed three times with PBS before being fluorescence imaged using an Olympus FV1000 laser confocal microscope (Japan). In the co-staining experiments, 1.0 μM of commercialized MitoTracker Green FM and 1.0 μM of **MNIR-H_2S** incubated together with cells for 30 min, washed three times with 10 mM of PBS, and then 40 μM of NaHS was added, and they were incubated for a further 30 min to carry out colocalization imaging analysis. The green channel was set to 500–560 nm, and the red channel was set to 640–680 nm, separately. The one-photon (OP) excitation wavelengths were set to 488 and 635 nm, respectively, and the two-photon (TP) excitation wavelength was set to 810 nm.

Nude mice aged 6–8 weeks were injected subcutaneously with 5 μM of **MNIR-H_2S** resolution (1% DMSO). In the control group, mice were injected with 5 μM of the resolution probe only, and NaHS was not used to resolve the images. In contrast, in the experimental group, the mice were injected with 5 μM of **MNIR-H_2S** resolution, and 40 μM of NaHS resolution was further used to resolve the images by a PhotoIMAGERTMRT imager with a 622 nm excitation filter and a 668 nm emission filter.

Results and discussion

In order to rationally design a TP-NIR fluorescent probe for sensing H_2S with organelle targeting properties, better biological imaging resolution, and deeper penetration depth, in this work, a TP excitation NIR emission mitochondria-targeting fluorescent probe **MNIR-H_2S** was constructed for sensing H_2S in living cells, onion tissue, zebrafish and nude mice. Its structure is shown in Fig. 1. Notably, an oxonium cation moiety serves as a mitochondrial targeting-group, an *o*-carboxyphenyl group is employed to occupy the 4-position of the oxonium cation to prevent the Michael addition reaction, and a well-known H_2S response site of DBN moiety acts as the H_2S "turn-on" moiety and the fluorescence intensity quenching group. Such a design affords an **MNIR-H_2S** probe with some excellent properties, such as TP excitation, NIR emission, mitochondrial localization, and so on. The route to synthesize **MNIR-H_2S** is shown in Fig. 1. Firstly, 2,4-dihydroxybenzaldehyde is reacted with methyl acetoacetate in EtOH to obtain 1 using piperidine as a catalyst; secondly, 2-(4-diethylamino-2-hydroxybenzoyl) benzoic acid is reacted with 1 in 98% H_2SO_4 at 90 °C to give 2; finally, 2 is reacted with 2,4-dinitrofluorobenzene in dry CH_2Cl_2 using triethylamine as a catalyst to give 3 (**MNIR-H_2S**). All compounds were characterized by NMR spectroscopy and mass spectrometry (see the ESI†).

With the **MNIR-H_2S** probe in hand, its spectral properties toward H_2S were measured in 10 mM of PBS (1% DMSO, pH = 7.4), as shown in Fig. 2. In this work, NaHS was chosen as the H_2S source. In the absence of H_2S, the **MNIR-H_2S** probe alone shows a characteristic absorption peak centered at 558 nm. While, in the presence of H_2S, the characteristic absorption band of **MNIR-H_2S** is red-shifted to 622 nm (a red shift of 64 nm), which matches well with the characteristic absorption band of fluorophore **2**. For the purpose of measuring the time-dependent fluorescence spectra of **MNIR-H_2S** toward 40 μM of NaHS in 10 mM of PBS (pH = 7.4, 1% DMSO) were used to study the sensitivity of the probe, and the fluorescence intensity was recorded at different times (0–10 min) (Fig. S1, ESI†). Subsequently, we measured the fluorescence response curve of **MNIR-H_2S** and different concentrations of H_2S in 10 mM of PBS (pH = 7.4), as shown in Fig. 2B. In the absence of H_2S, the solution of **MNIR-H_2S** exhibited almost no fluorescence intensity signal at 668 nm. While in the presence of H_2S, with increasing NaHS concentration (0–50 μM), the fluorescence intensity rapidly and significantly enhanced at 668 nm, accompanied by a color change from yellow to blue (Fig. 1E and F). Therefore, **MNIR-H_2S** displayed good colorimetric and fluorescence response to H_2S. Notably, a linear correlation between the fluorescence intensity ratio I_0/I_{668} and H_2S concentrations in the range of 0–5 μM was obtained (Fig. 2D), and the detection limit of **MNIR-H_2S** response to

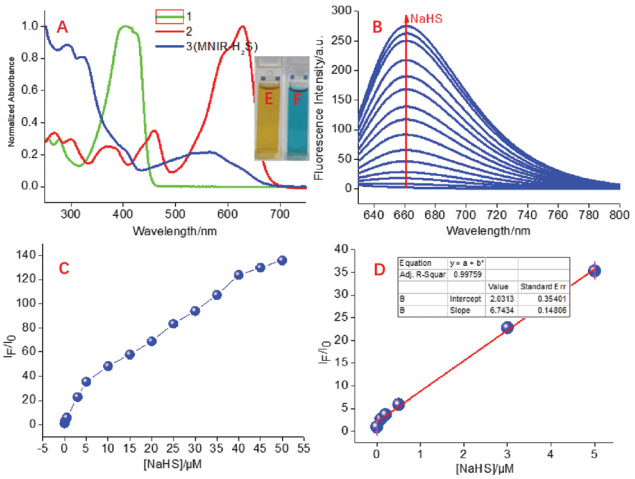

Fig. 2 (A) The normalized absorbance spectra of 1, 2, and **MNIR-H$_2$S**; (B) fluorescence response spectra of **MNIR-H$_2$S** (1.0 μM) with varied concentrations of NaHS (0–50.0 μM), λ_{ex} = 622 nm; (C) calibration curve of **MNIR-H$_2$S** toward NaHS (0–50.0 μM); (D) linear response of 1.0 μM of **MNIR-H$_2$S** and 0–5.0 μM of NaHS in 10 mM of PBS buffer (1% DMSO); (E, F) the insets show the change in the color of the **MNIR-H$_2$S** probe before and after adding 50.0 μM of H$_2$S into 1.0 μM of **MNIR-H$_2$S**, where the photographs were obtained under visible light.

H$_2$S was calculated to be as low as 14.8 nM (Fig. 2D) according to the 3σ/slope. Therefore, **MNIR-H$_2$S** can be used as a potential fluorescence probe with outstanding properties for the sensing of H$_2$S in living biological systems.

To examine the selectivity, we incubated **MNIR-H$_2$S** with different types of cations, anions, common amino acids and biothiols at 100 μM, such as cysteine (Cys), glutathione (GSH), Na^+, ascorbic acid (vitamin C), K^+, Ca^{2+}, Mg^{2+}, Fe^{3+}, Zn^{2+}, Cu^{2+}, H$_2$S, Glycine (Gly), Blank, Glucose (Glu), and Pb^{2+}, respectively. As shown in Fig. 3A and Fig. S2 (ESI†), in the presence of H$_2$S, when excited with an excitation wavelength of 622 nm, H$_2$S can induce a robust fluorescence intensity enhancement at 668 nm, while in the presence of100 μM of the other analyzed species only slight changes can be observed, meaning that their influence can be ignored. The results suggest that **MNIR-H$_2$S** shows excellent selectivity and a specific response toward H$_2$S over other analyzed species. Following this, fluorescence responses of **MNIR-H$_2$S** (1 μM) to H$_2$S at different pH values were also studied (Fig. 3B). The experimental results exhibited that in the absence of hydrogen sulfide, the pH of the solution changed from 3.0 to 8.0, with almost no change in fluorescence intensity at 668 nm being observed, and when **MNIR-H$_2$S** was incubated with hydrogen sulfide in solutions of different pH values (3.0–8.0), the fluorescent intensity showed significant changes at 668 nm. Moreover, according to the experimental results, the optimal pH range for the reaction of **MNIR-H$_2$S** with hydrogen sulfide was determined as 6.0–8.0, showing that **MNIR-H$_2$S** is suitable for use in biological applications at physiological pH. Thus, 10 mM of pH 7.4 PBS solution was used in all of the experiments.

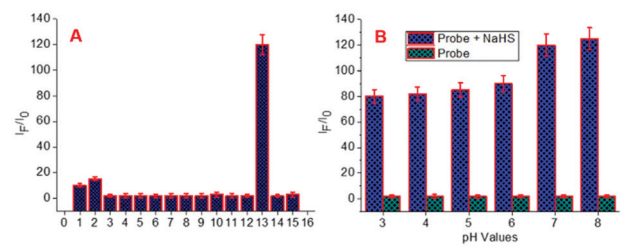

Fig. 3 (A) Selectivity experiments: 1 μM of **MNIR-H$_2$S** incubated with various analyzed species/NaHS (100 μM of other species and 40 μM of NaHS) in PBS buffer (10 mM, pH = 7.4, water/DMSO = 99/1, v/v), λ_{ex} = 622 nm, legend: (1) GSH, (2) Cys, (3) Vitamin C, (4) K^+, (5) Ca^{2+}, (6) Na^+, (7) Mg^{2+}, (8) Zn^{2+}, (9) Fe^{3+}, (10) Gly, (11) Cu^{2+}, (12) Blank, (13) H$_2$S, (14) Pb^{2+}, (15) Glu; (B) The effect of different pH values (3.0–8.0) on the response of 1 μM of **MNIR-H$_2$S** and hydrogen sulfide, blue columns: in the presence of NaHS (40 μM), blue-green columns: in the absence of NaHS. Each experiment was repeated three times, λ_{ex} = 622 nm.

Encouraged by the above results, we evaluated the biological application of **MNIR-H$_2$S** in the imaging of H$_2$S in living cells. First, we investigated the cytotoxicity of **MNIR-H$_2$S** by MTT (Fig. S3, ESI†). When HeLa cells were incubated with 0–12 μM of the probe, the cell viability did not decrease significantly, indicating that **MNIR-H$_2$S** shows low cytotoxicity to living cells under physiological conditions and is suitable for biological application. Subsequently, we investigated the feasibility of using **MNIR-H$_2$S** for the sensing H$_2$S in living HeLa cells. HeLa cells were incubated with **MNIR-H$_2$S** and showed weak fluorescence in the red channel (Fig. 4A: a and b) upon excitation at 635 nm. The HeLa cells were stained with 1 μM of **MNIR-H$_2$S** for 30 min, washed three times with 10 mM of PBS to remove any excess probe, and were then further incubated with 40 μM of NaHS for 30 min to detect H$_2$S (Fig. 4A: c and d), where the fluorescence intensity was bright in the red channel. This result shows that **MNIR-H$_2$S** can be applied in the imaging of H$_2$S in living HeLa cells.

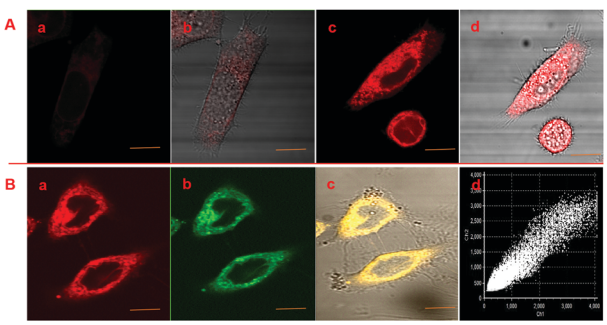

Fig. 4 (A) Confocal images of HeLa cells treated with **MNIR-H$_2$S** for detecting H$_2$S: (a) HeLa cells incubated with only **MNIR-H$_2$S** in the fluorescence image of the red channel excited at 635 nm; (b) an overlay image of (a) and bright field imaging; (c) HeLa cells treated with **MNIR-H2S**, following treatment with NaHS (40 μM) for red channel imaging excited at 635 nm; (d) an overlay image of (c) and bright field imaging. (B) Mitochondria co-localization images of **MNIR-H$_2$S** in HeLa cells: (a) **MNIR-H$_2$S** (1 μM, red channel, λ_{ex} = 635 nm, λ_{em} = 640–680 nm) for 30 min, following treatment with NaHS (40 μM) for 30 min for the red channel imaging; (b) cells incubated with MitoTracker Green FM (1 μM, green channel, λ_{ex} = 488 nm, λ_{em} = 500–560 nm) for the green channel imaging; (c) overlay image of (a), (b) and the bright field imaging; (d) the correlation of **MNIR-H$_2$S** and MitoTracker Green FM intensities. Scale bar: 20 μm.

For the purpose of verifying that **MNIR-H_2S** can target the mitochondria for the sensing of H_2S, HeLa cells were co-stained with 1 μM of **MNIR-H_2S** and 1 μM of MitoTracker Green (FM) for 30 min, and then washed three times with 10 mM of PBS (pH7.4) to remove the excess **MNIR-H_2S** and FM, and were then further incubated with 40 μM of NaHS for 30 min to carry out fluorescence imaging. As shown in Fig. 4B, the confocal laser scanning microscopy results show that **MNIR-H_2S** exhibits red fluorescence intensity around the perinuclear areas in the cytoplasm upon excitation at 635 nm. The co-localization and colorimetric assays with MitoTracker Green FM were observed with a high correlation coefficient of 0.95 (Fig. 4B: a), indicating that **MNIR-H_2S** is membrane permeable and capable of the fluorescence imaging of mitochondrial H_2S in living cells.

We further evaluated the biological application of **MNIR-H_2S** in the imaging of H_2S in living tissues and zebrafish from TP images (δ_{TPA} = 40 GM, λ_{ex} = 810 nm, Table S1, ESI†). First, **MNIR-H_2S** was applied to onion tissue slices. The onion tissue slices were stained with 1 μM **MNIR-H_2S** for 30 min, and subsequently stimulated without or with 40 μM NaHS for 30 min to carry out fluorescence imaging, where the red fluorescence intensity in the tissues was observed by multiphoton confocal microscopy (Olympus, FV1000) in z-scan mode, which showed that **MNIR-H_2S** is capable of tissue imaging at depths of 90 and 95 μm (Fig. 5A and B) by 2PFM imaging, and possesses good tissue penetration. Next, **MNIR-H_2S** was used to carry out fluorescence imaging in a zebrafish model. 5 Day-old vertebrate zebrafish were chosen as the experimental samples, which were divided into control and experimental groups. For the control group, in the absence of NaHS, the zebrafish showed dim fluorescence intensity in the red channel (Fig. 5C). While, for the experimental group, in the presence of 40 μM NaHS for 30 min, and then subsequently being incubated with **MNIR-H_2S** for 30 min, the fluorescence intensity was obviously enhanced in the red channel (Fig. 5D), which exhibited that the **MNIR-H_2S** probe has the capacity to image H_2S in living tissues and zebrafish.

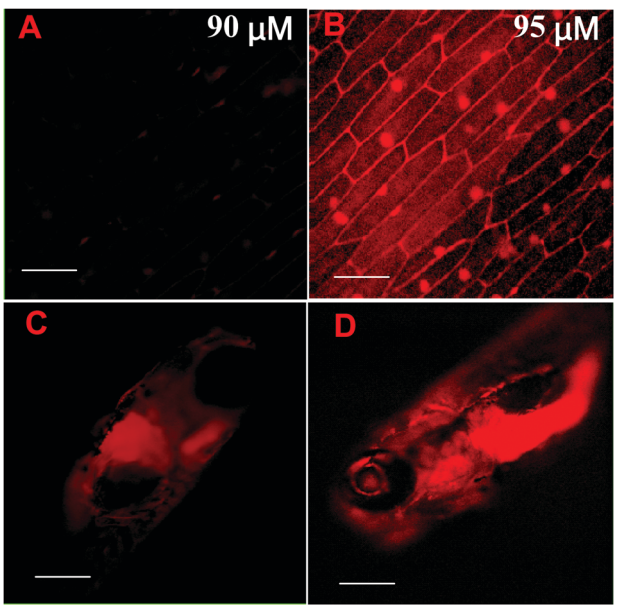

Fig. 5 The fluorescence imaging of onion tissue and zebrafish incubated with **MNIR-H_2S** (1 μM) for 30 min, and then without or with continued treatment with NaHS (40 μM) for 30 min for imaging. (A) Treatment with only **MNIR-H_2S** for onion tissue imaging; (B) treatment with **MNIR-H_2S** and NaHS for onion tissue imaging; (C) treatment with only **MNIR-H_2S** for zebrafish imaging; (D) treatment with **MNIR-H_2S** and NaHS for zebrafish imaging. λ_{ex} = 810 nm, λ_{em} = 640–680 nm, scale bar: 100 μm.

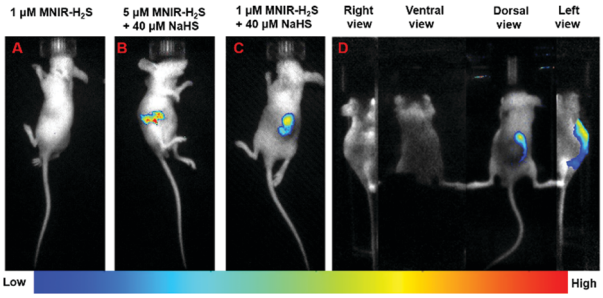

Fig. 6 Representative fluorescence images (rainbow color) for anesthetized nude mice subcutaneously injected with **MNIR-H_2S** (1 μM) or **MNIR-H_2S** (1 or 5 μM) and NaHS (40 μM). (A) Control experiments: injected with **MNIR-H_2S** (1 μM); (B) after injecting with **MNIR-H_2S** (5 μM) and NaHS (40 μM) 10 min for imaging; (C) after injecting with **MNIR-H_2S** (1 μM) and NaHS (40 μM) 10 min for imaging; (D) after injecting with **MNIR-H_2S** (1 μM) and NaHS (40 μM) 10 min for simultaneous 4-view imaging.

Finally, the **MNIR-H_2S** probe was further applied for the 4-view fluorescence imaging of H_2S in living nude mice. After intraperitoneal injection of 1 μM or 5 μM of **MNIR-H_2S** into the living mice, 40 μM of NaHS solutions were further injected to trigger fluorescence intensity, and a bright fluorescence intensity was observed from the mice (Fig. 6B), and 1 μM of probe **MNIR-H_2S** together with 40 μM of NaHS solution triggered a relatively dim fluorescence intensity enhancement in the mice (Fig. 6C). The images show that **MNIR-H_2S** exhibits high resolution for bioimaging. In order to further eliminate false positives, we adopted a 4-view mode for imaging (Fig. 6D). These results demonstrate that the probe possesses high penetration capability in animals for the fluorescence imaging of H_2S.

Conclusions

In summary, in this work, we have reported a new mitochondria-targeting two-photon in near-infrared out probe **MNIR-H_2S**. In this probe, an oxonium cation acts as a mitochondria-targeting group, while a hydroxyl group is linked to a DNB group as a hydrogen sulfide response moiety, which affords the **MNIR-H_2S** probe with good selectivity and high sensitivity towards H_2S. The constructed probe was successfully applied in "turn-on" fluorescence intensity for the sensing of H_2S in HeLa cells, onion tissue, zebrafish, and nude mice. Therefore, we hope that **MNIR-H_2S** can be used as a robust tool with potential biological applications for imaging of the gaseous signalling molecule H_2S in biological systems.

Live subject statement

All animal procedures were performed in accordance with the Guidelines for Care and Use of Laboratory Animals of Central

South University of Forestry and Technology and approved by the Animal Ethics Committee of Central South University of Forestry and Technology.

Conflicts of interest

There are no conflicts to declare.

Acknowledgements

This work was supported by the Natural Science Foundation of China (NSFC, Grants 21605046, 32060144), the Hunan Provincial Natural Science Foundation of China (No. 2017JJ3060), and the Science and Technology Innovation Platform and Talent Project of Hunan Province (2017TP1021, 2018JJ3117).

References

1 (*a*) E. Culotta and D. E. Koshland, *Science*, 1992, **258**, 1862; (*b*) T. Morita, M. A. Perrella, M. E. Lee and S. Kourembanas, *Proc. Natl. Acad. Sci. U. S. A.*, 1995, **92**, 1475.

2 (*a*) H. Kimura, *Exp. Physiol.*, 2011, **96**, 833; (*b*) H. Kimura, *Amino Acids*, 2011, **41**, 113; (*c*) B. D. Paul and S. H. Snyder, *Nat. Rev. Mol. Cell Biol.*, 2012, **13**, 499; (*d*) J. E. Dominy and M. H. Stipanuk, *Nutr. Rev.*, 2004, **62**, 348.

3 S. Fiorucci, E. Antonelli, A. Mencarelli, S. Orlandi, B. Renga, G. Rizzo, E. Distrutti, V. Shah and A. Morelli, *Hepatology*, 2005, **42**, 539.

4 D. J. Lefer, *Br. J. Pharmacol.*, 2008, **155**, 617.

5 P. Kamoun, M. C. Belardinelli, A. Chabli, K. Lallouchi and B. Chadefaux-Vekemans, *Am. J. Med. Genet.*, 2003, **116A**, 310.

6 K. Eto, T. Asada, K. Arima, T. Makifuchi and H. Kimura, *Biochem. Biophys. Res. Commun.*, 2002, **293**, 1485.

7 (*a*) T. Zhou, Y. Yang, K. Zhou, M. Jin, M. Han, W. Li and C. Yin, *Sens. Actuators, B*, 2019, **301**, 127116; (*b*) J. Wang, Y. Wen, F. J. Huo and C. Yin, *Sens. Actuators, B*, 2019, **297**, 126773; (*c*) Y. Chen, C. Zhu, Z. Yang, J. Chen, Y. He, Y. Jiao, W. He, L. Qiu, J. Cen and Z. Guo, *Angew. Chem.*, 2013, **125**, 1732; (*d*) X. Zhang, H. Tan, Y. Yan, Y. Hang, F. Yu, X. Qu and J. Hua, *J. Mater. Chem. B*, 2017, **5**, 2172; (*e*) A. Ji, Y. Fan, W. Ren, S. Zhang and H. W. Ai, *ACS Sens.*, 2018, **3**, 992; (*f*) Y. L. Pak, J. Li, K. C. Ko, G. Kim, J. Y. Lee and J. Yoon, *Anal. Chem.*, 2016, **88**, 5476.

8 M. H. Lee, J. S. Kim and J. L. Sessler, *Chem. Soc. Rev.*, 2015, **44**, 4185.

9 (*a*) W. Sun, J. Fan, C. Hu, J. Cao, H. Zhang, X. Xiong, J. Wang, S. Cui, S. Sun and X. Peng, *Chem. Commun.*, 2013, **49**, 3890; (*b*) H. M. Kim and B. R. Cho, *Chem. Rev.*, 2015, **115**, 5014; (*c*) S. K. Bae, C. H. Heo, D. J. Choi, D. Sen, E. H. Joe, B. R. Cho and H. M. Kim, *J. Am. Chem. Soc.*, 2013, **135**, 9915.

10 (*a*) L. Pan, S. Sun, L. Zhang, K. Jiang and H. Lin, *Nanoscale*, 2016, **8**, 17350; (*b*) Y. Lv, M. Liu, Y. Zhang, X. Wang, F. Zhang, F. Li, W. E. Bao, J. Wang, Y. Zhang, W. Wei, G. Ma, L. Zhao and Z. Tian, *ACS Nano*, 2018, **12**, 1350; (*c*) Z. Mao, H. Jiang, X. Song, W. Hu and Z. Liu, *Anal. Chem.*, 2017, **89**, 9620.

11 (*a*) J. Liu, Y. Q. Sun, J. Zhang, T. Yang, J. Cao, L. Zhang and W. Guo, *Chem. – Eur. J.*, 2013, **19**, 4717; (*b*) Y. Yang, L. He, K. Xu and W. Lin, *New J. Chem.*, 2019, **43**, 10926; (*c*) L. Zhou, D. Lu, Q. Wang, S. Liu, Q. Lin and H. Sun, *Biosens. Bioelectron.*, 2017, **91**, 699; (*d*) L. Yuan, W. Lin and H. Chen, *Biomaterials*, 2013, **34**, 9566.

12 (*a*) T. Liu, Z. Xu, D. R. Spring and J. Cui, *Org. Lett.*, 2013, **15**, 2310; (*b*) L. Yang, Y. Su, Y. Geng, Y. Zhang, X. Ren, L. He and X. Song, *ACS Sens.*, 2018, **3**, 1863.

13 (*a*) M. Fang, R. Adhikari, J. Bi, W. Mazi, N. Dorh, J. Wang, N. Conner, J. Ainsley, T. G. Karabencheva-Christova, F. T. Luo, A. Tiwari and H. Liu, *J. Mater. Chem. B*, 2017, **5**, 9579; (*b*) Š. Starčević, P. Brožič, S. Turk, J. Cesar, T. L. Rižner and S. Gobec, *J. Med. Chem.*, 2011, **54**, 248.

